C_n-symmetric higher-order topological crystalline insulators in atomically thin transition metal dichalcogenides

Shifeng Qian, Gui-Bin Liu, Cheng-Cheng Liu,[*] and Yugui Yao

Centre for Quantum Physics, Key Laboratory of Advanced Optoelectronic Quantum Architecture and Measurement (MOE),
School of Physics, Beijing Institute of Technology, Beijing 100081, China
and Beijing Key Lab of Nanophotonics & Ultrafine Optoelectronic Systems, School of Physics, Beijing Institute of Technology,
Beijing 100081, China

Based on first-principles calculations and symmetry analysis, we predict atomically thin ($1 - N$ layers) $2H$ group-VIB transition metal dichalcogenides (TMDs) MX_2 (M = Mo, W; X = S, Se, Te) are large-gap higher-order topological crystalline insulators (HOTCIs) protected by C_3 rotation symmetry. We explicitly demonstrate the nontrivial topological indices and the existence of hallmark corner states with quantized fractional charge for these familiar TMDs with a large bulk optical band gap (1.64–1.95 eV for the monolayers), which would facilitate the experimental verification and exploration of the HOTCI states. Furthermore, we find that the well-defined corner states exist in the triangular finite-size flakes with armchair edges of the atomically thin ($1 - N$ layers) $2H$ group-VIB TMDs, and the corresponding quantized fractional charge is the number of layers N modulo three. The fractional corner charge will double when spin degree of freedom is taken into account.

I. INTRODUCTION

Atomically thin two-dimensional (2D) transition metal dichalcogenide (TMD) semiconductors have attracted great scientific and technological interest because of their extraordinary properties, such as the direct band gap in the visible frequency range, remarkable optical properties, and rich valley-related physics [1–7]. Among various TMDs, the group-VIB ones MX_2 (M = Mo, W; X = S, Se, Te) have been most extensively studied in 2D forms, where both the monolayers and few-layers are proved to be stable in air at room temperature except MTe$_2$.

Exploring new topological quantum states, especially high-order topological crystal insulator (HOTCI) states, and discovering good candidate materials are among the most active studies in condensed matter physics and materials science [8–27]. Different from a conventional TCI having protected gapless states on its symmetric boundaries with one dimension lower than the bulk, HOTCIs feature the lower-dimensional protected boundary states. For instance, three dimensional (3D) second-order TCIs host one-dimensional (1D) gapless states along their hinges, and 2D HOTCIs display in-gap corner modes. A few theoretical materials for 3D and 2D HOTCIs were proposed in the literature [28–41]. However, second-order TCIs have only been experimentally observed in 3D single crystal bismuth [42] and some artificial systems [43–54]. Therefore, proposing and discovering ideal and real material candidates of 2D HOTCIs are still urgent and important.

We put forward guidelines for designing the 2D HOTCI state in hexagonal lattices with s and p orbitals, and predicted abundant material candidates [40], recently. In this work we generalize to the systems of d orbitals, among which the atomically thin group-VIB TMDs (monolayers, bilayers, few-layers, etc.) are most representative. The band topology of the $2H$ bilayer group-VIB TMDs MX_2 (M = Mo, W; X = S, Se, Te) with inversion symmetry (P) and time-reversal symmetry (T) could be characterized by the second Stiefel-Whitney invariant w_2 [55]. Although w_2 is zero for the bilayers, there are still nonzero topological index and corner states with quantized fractional charge protected by C_3 rotation symmetry localized at the corners of the $2H$ bilayer group-VIB TMDs, indicating a HOTCI, by combined density function
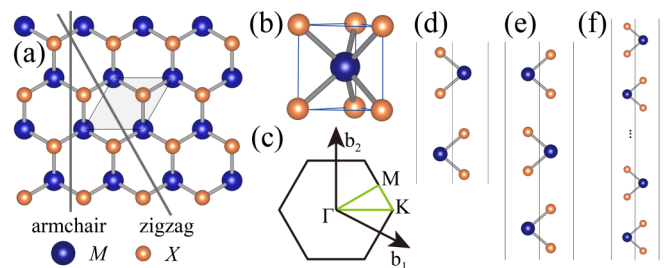

FIG. 1. (a) Top view of transition metal dichalcogenides MX_2 (M = Mo, W; X = S, Se, Te) monolayer. The blue and orange spheres represent M and X atoms, respectively. The light gray diamond region is the unit cell of MX_2. The gray lines mark the zigzag and armchair edges. (b) Trigonal prismatic coordination geometry of MX_2. (c) The first Brillouin zone with high-symmetric points. $\mathbf{b_1}$ and $\mathbf{b_2}$ are the reciprocal lattice vectors. (d)–(f) Side view of bilayer, trilayer, and multilayer MX_2 of $2H$ stacking.
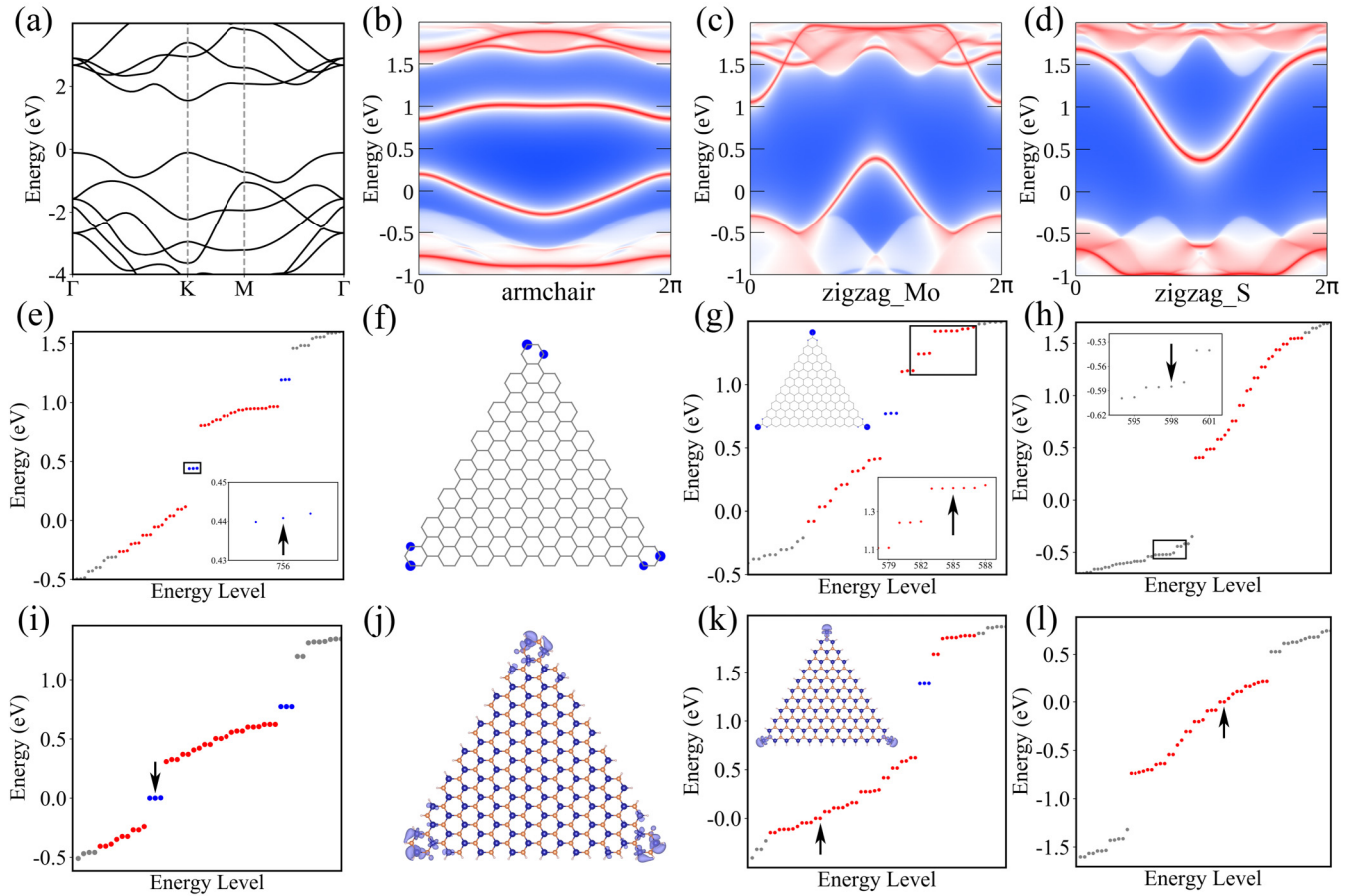
*ccliu@bit.edu.cn

FIG. 2. (a) Bulk band of monolayer MoS_2. (b)–(d) The edge states of three semi-infinite planes with respective armchair, zigzag_Mo, and zigzag_S edges, calculated by the Wannier interpolation method. (e) The energy spectra of a triangular nanoflake (f) with armchair edges calculated by the Wannier interpolation method. The gray, red, and blue dots in (e) stand for the respective bulk, edge, and corner states. The arrow in the zoomed rectangle marks the position of the Fermi level by electron counting. The real-space distribution of the corner states framed by a rectangle is plotted in (f). (g) The energy spectra of a triangular nanoflake with zigzag_Mo edges calculated by the Wannier interpolation method. Although there are still corner states in blue located at the corners, the Fermi level marked by an arrow and determined by electron counting is in the edge states in red, indicating an intrinsic metallic edge state. (h) The energy spectra of a triangular nanoflake with zigzag_S edges calculated by the Wannier interpolation method. There are no in-gap corner states, and the Fermi level labeled by an arrow is located in the bulk states, signing an intrinsic metallic bulk state. (i) The energy spectrum of a triangular nanoflake at armchair edges with hydrogen passivation consisting of 108 Mo atoms, 216 S atoms, and 96 H atoms calculated by VASP. (j) The real-space distribution of the corner states in (i). (k) The energy spectrum of a triangular nanoflake at zigzag_Mo edges with hydrogen passivation consisting of 78 Mo atoms, 132 S atoms, and 72 H atoms calculated by VASP. The inset shows the real-space distribution of the corner states. (l) The energy spectrum of a triangular nanoflake at zigzag_S edges with hydrogen passivation consisting of 66 Mo atoms, 156 S atoms, and 72 H atoms calculated by VASP. The arrows in (i), (k), and (l) label the Fermi level.

theory (DFT) simulation and symmetry analysis. Actually, this HOTCI state protected by rotation symmetry does not need P but C_3, which is owned by all other $2H$ few-layer group-VIB TMDs (monolayers, trilayers, quadlayers, etc.). We find such few-layer TMDs are also large-gap HOTCIs protected by C_3 symmetry. These atomically thin group-VIB TMDs MX_2 ($M =$ Mo, W; $X =$ S, Se, Te) have a large bulk optical band gap (e.g., 1.64–1.95 eV for the monolayers), which would facilitate the experimental detection by scanning tunneling microscopy (STM).

II. TOPOLOGICAL CLASSIFICATION

The bulk of group-VIB TMDs with $2H$ stacking crystalizes in space group D_{6h}^4 with inversion symmetry. For

the atomically thin counterparts, the symmetry is reduced to D_{3h} (monolayers), D_{3d} (bilayers), D_{3h} (trilayers), and D_{3d} (quadlayers), as shown in Fig. 1. The inversion symmetry is preserved in the even-layer films (D_{3d}), but broken in the odd-layer ones (D_{3h}). First, we take into account the centrosymmetric spinless bilayer, with spin-orbital coupling (SOC) discussed later. The higher-order band topology of spinless systems with PT symmetry can be characterized by the so-called second Stiefel-Whitney number w_2 (see details in the Supplemental Material [55]). We take bilayer MoS_2 as an example, and calculate the second Stiefel-Whitney number w_2, and find $w_2 = 0$ [Fig. 3(b)], which is also checked by using the parity criterion and nested Wilson loop (see Supplemental Material [55]), seeming to indicate a trivial state. However, we still found the nontrivial topological indices and
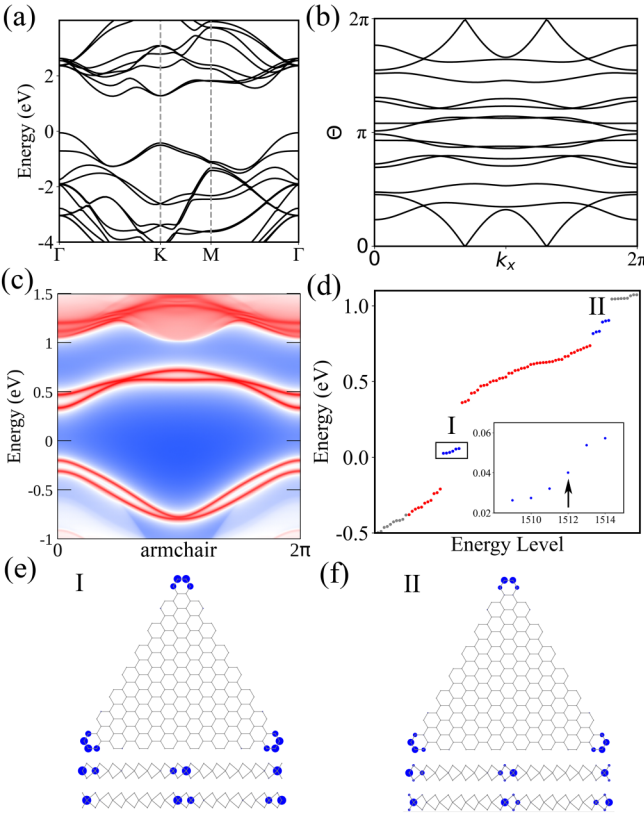
FIG. 3. (a,c) Bulk band and armchair edge states of bilayer MoS$_2$. (b) Wilson loop of bilayer MoS$_2$. The number of crossings on $\theta = \pi$ is zero, indicating the $w_2 = 0$. (d) Energy spectrum of a triangular finite-size flake of bilayer MoS$_2$ calculated from the Wannier interpolation method. The gray, red, and blue dots mark the respective bulk, edge, and corner states. The corner states are split in two groups labeled by I and II in different energy regions. The arrow denotes the Fermi level by valence electron counting. (e,f) The top view and side view of the real-space distribution of the two groups of the corner states.

the hallmark corner states with fractional charge protected only by C_3 symmetry in the bilayer.

The nontrivial topological indices and hallmark corner states with quantized fractional charge can be described by the C_3-symmetry eigenvalues of the occupied energy bands at the high-symmetric points of the Brillouin zone (BZ) [63]. The three-fold rotation symmetry eigenvalues at the high-symmetric points $\mathbf{\Sigma}^{(3)}$ in the BZ is denoted as $\Sigma_m^{(3)} = e^{2\pi i(m-1)/3}$, for $m = 1, 2, 3$. The topological invariants can be defined through the rotation eigenvalues at $\mathbf{\Sigma}^{(3)}$ compared to a certain reference point $\mathbf{\Gamma} = (0, 0)$, i.e., $[\Sigma_m^{(3)}] \equiv \#\Sigma_m^{(3)} - \#\Gamma_m^{(3)}$, where $\#\Sigma_m^{(3)}$ ($\#\Gamma_m^{(3)}$) is the number of occupied bands with eigenvalue $\Sigma_m^{(3)}$ ($\Gamma_m^{(3)}$). The topological indices $\chi^{(3)}$ and fractional corner charge $Q_{corner}^{(3)}$ for C_3-symmetric HOTCIs read

$$\chi^{(3)} = \left([K_1^{(3)}], [K_2^{(3)}]\right),$$
$$Q_{corner}^{(3)} = \frac{e}{3}[K_2^{(3)}] \bmod e, \tag{1}$$

where the superscript 3 of $\chi^{(3)}$ and $Q_{corner}^{(3)}$ labels the C_3 symmetry, and e is the charge of a free electron.

III. HOTCIS IN MONOLAYER GROUP-VIB TMDs PROTECTED BY C_3 SYMMETRY

The above C_n symmetry protected HOTCI mechanism can directly apply to the monolayer ones. For the monolayer MoS$_2$, the nonzero topological index $\chi^{(3)} = (-2, 1)$ in a $\sqrt{3} \times \sqrt{3}$ supercell and the fractional corner charge $Q_{corner}^{(3)} = e/3$. Figure 2(a) shows the bulk band structure of monolayer MoS$_2$. As plotted in Fig. 1(a), one usually cuts the group-VIB TMDs MX_2 with armchair and zigzag edges, and the zigzag edge has two versions differentiated by M or X termination, labeled by zigzag_M and zigzag_X. As shown in Fig. 2, we construct three semi-infinite planes and three triangular finite-size flakes with armchair, zigzag_M, and zigzag_X edges, respectively. There are two gapped armchair edge states in the bulk gap, as shown in Fig. 2(b). The edge states for zigzag_Mo and zigzag_S are plotted in Figs. 2(c) and 2(d).

To explicitly reveal the hallmark corner states, we calculate the energy spectrum of the three triangular nanoflakes with three different edges based on the Wannier interpolation method, as shown in Figs. 2(e) to 2(h). For the armchair nanoflake, in the middle of the edge states exit three degenerate states [blue dots in Fig. 2(e)], whose charge real-space distribution is plotted in Fig. 2(f). Such three states are well located at the three corners of the flake [Fig. 2(f)], i.e., the corner states. We consider (Mo:$5s^1 4d^5$) and (S:$3p^4$) as the valence electron configuration of MoS$_2$ in Wannier functions construction. In the monolayers, one unit cell has one Mo atom and two S atoms, so the number of the valence electrons is $(6 + 2 \times 4)/2 = 7$, where the divisor 2 denotes the spinless case. The triangular armchair flake consists of 108 unit cells, and has $108 \times 7 = 756$ valence electrons. The Fermi level is determined by the electron counting and indicated by an arrow [Fig. 2(e)]. The other group-VIB TMDs have the similar valence electron configuration and valence electron counting. As for the two zigzag nanoflakes, the Fermi level lies in the edge or bulk states with the hallmark corner states buried, as shown in Figs. 2(g) and 2(h). We would like to stress that only the armchair flakes have appropriate electron filling, i.e., with corner states at the Fermi level, while the nanoflakes with the two kinds of zigzag edges have metallic bulk or edge states. Therefore, we are mainly interested in the 1D or zero-dimensional (0D) samples with armchair edges for the group-VIB TMDs MX_2.

While these effects from the edge deformation and dangling bonds may result in the overlap of the corner states with edge states or bulk states, one can eliminate these effects by surface modification, such as by passivating the edges with hydrogen atoms. We perform DFT calculation on the energy spectra of monolayer MoS$_2$ flakes with the three different edges with hydrogen passivation calculated by Vienna *ab initio* simulation package (VASP), as shown in Figs. 2(i), 2(j), 2(k), and 2(l). The energy spectra of the other monolayer TMDs armchair flakes with hydrogen passivation calculated by VASP are given in Figs. S1 to S5 [55]. The results obtained by VASP are similar with those by the Wannier interpolation method. We directly calculate the corner charge of MoS$_2$ armchair nanoflake passivated with hydrogen atoms by VASP, and find the accumulation charge mod e at each corner is $0.30e$, which is close to the theoretical value $e/3$. The details
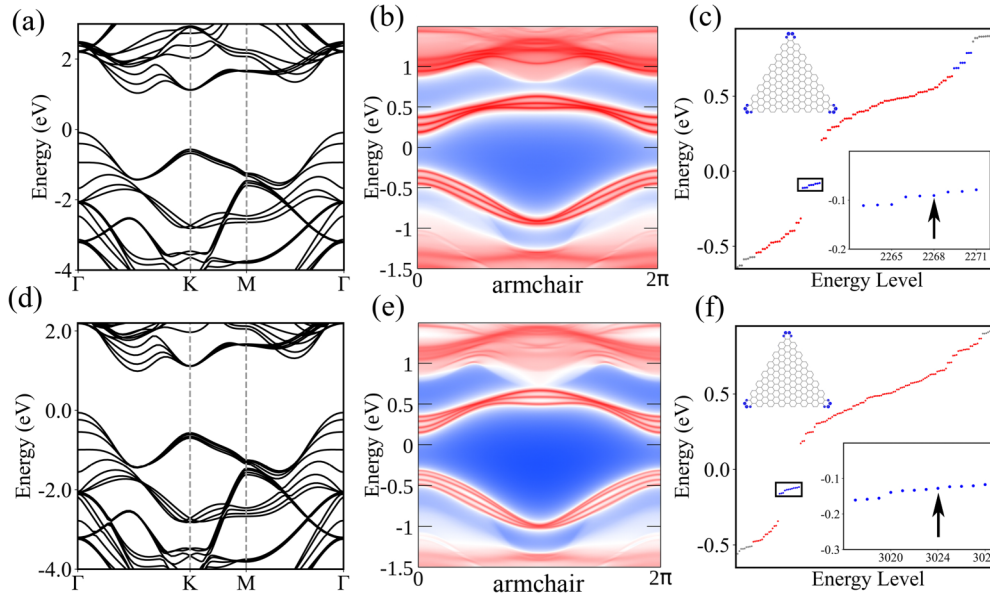
FIG. 4. (a,d) Bulk band structures of trilayer and quadlayer MoS$_2$. (b,e) Armchair edge states of trilayer and quadlayer MoS$_2$. Energy discrete spectra of the finite-size triangular flakes of (c) trilayer and (f) quadlayer MoS$_2$ calculated from the Wannier interpolation method. The blue states in (c) and (f), whose charge real-space distribution is plotted in the insets, are well localized at the corners. The gray, red, and blue dots represent the respective bulk, edge, and corner states. The Fermi level marked by the arrows in (c) and (f) is determined by electron counting.

are presented in Appendix A. The other monolayer group-VIB TMDs are also HOTCIs (see details in Supplemental Material [55]).

IV. HOTCIS IN 2H BILAYER GROUP-VIB TMDS WITH PT AND C_3 SYMMETRIES

The topological index of bilayer MoS$_2$ $\chi^{(3)} = (-4, 2)$ and the fractional corner charge $Q_{corner}^{(3)} = 2e/3$. The bulk band structure and armchair edge states of bilayer MoS$_2$ are plotted in Figs. 3(a) and 3(c). To explore the hallmark corner states of bilayer MoS$_2$, we calculate the energy spectrum of a triangular finite-size flake [Fig. 3(d)]. By similar electron counting as that of the monolayer, we fix the position of the Fermi level, just right at the blue corner states, marked by an arrow in the zoomed rectangle in Fig. 3(d). There are two groups of states in blue, with one group near zero energy in the spectrum and the other with higher energy, labeled as I and II. For the group I, the top view and side view of the real-space distribution of the six states are shown in Fig. 3(e). From the top view, one can see these states are well located at the corners of the flake, corresponding to the corner states. From the side view, these corner states are evenly distributed on two layers, and mainly on the Mo atoms. Figure 3(f) shows the top view and side view of the real-space distribution of the group II, with the similar distribution as that of the group I. The analogous analysis and results for the other bilayer group-VIB TMDs are given in the Supplemental Material [55].

V. HOTCIS IN OTHER FEW-LAYER AND MULTILAYER GROUP-VIB TMDS PROTECTED BY C_3 SYMMETRY

Figures 4(a) and 4(d) show the bulk band structures of trilayer and quadlayer MoS$_2$. Their armchair edge states are plotted in Figs. 4(b) and 4(e). The discrete energy spectra of

two triangular finite-size flakes of the trilayer and quadlayer are shown in Figs. 4(c) and 4(f). One can see the well-defined corner states are located at the corners of the both flakes. According to Eq. (1), the fractional corner charge of the quadlayer nanoflake is $Q_{corner}^{(3)} = e/3$. In spite of the clear corner states for the trilayer nanoflake, the corner charge is zero. In the trilayer (or six, nine, etc., layers) nanoflake, the original corner states with $e/3$ fractional corner charge in each layer will mix together with an integer corner charge remaining, thus without fractional corner charge. The few-layer TMDs which are the stacking of monolayers by weak van der Waals-like forces are natural but not trivial promotions of the monolayer ones. Based on the above analysis, we propose a simple formula to calculate the fractional corner charge of the few-layer TMDs, which reads

$$Q_N^{corner} = e\frac{N}{3} \bmod e, \qquad (2)$$

where N is the number of layers. The number of the corner modes at one corner of the flake equals the number of layers. The similar analysis and results hold for the other trilayer and quadlayer group-VIB TMDs [55] as well as the other multilayer group-VIB TMDs (Appendix B).

VI. EFFECT OF SPIN-ORBITAL COUPLING

The fractional corner charge in the 2D system with SOC can also be classified by rotation symmetry [28]. The topological indices $\chi_{SOC}^{(3)}$ and fractional corner charge $Q_{SOC}^{(3)}$ for C_3-symmetry protected HOTCIs with SOC read

$$\chi_{SOC}^{(3)} = ([\tilde{K}_1^{(3)}], [\tilde{K}_2^{(3)}]),$$
$$Q_{SOC}^{(3)} = \frac{2e}{3}([\tilde{K}_1^{(3)}] + [\tilde{K}_2^{(3)}]) \bmod 2e, \qquad (3)$$

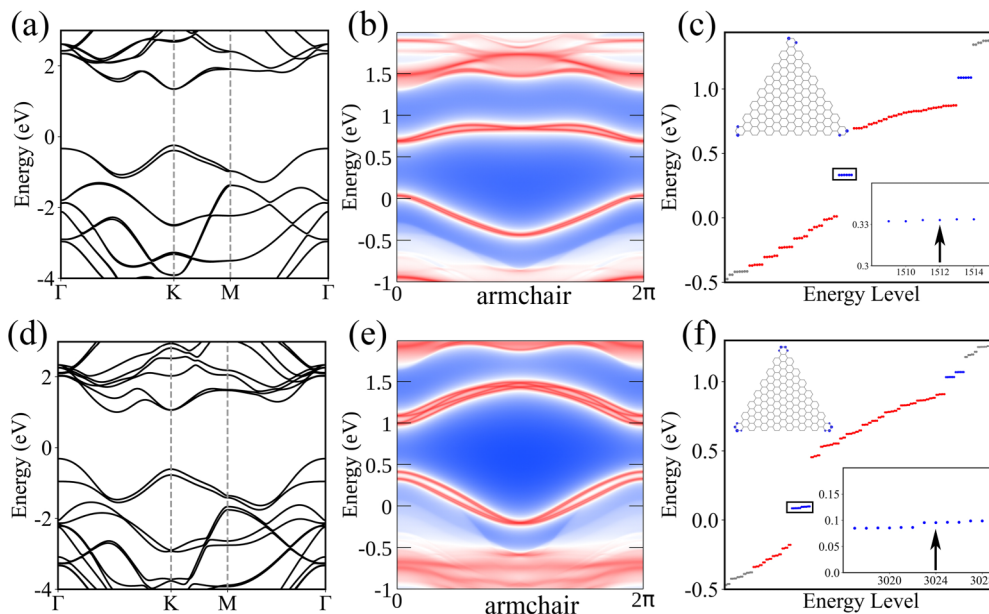where $\tilde{K}_{i=1,2,3}^{(3)} = \{e^{i\pi/3}, -1, e^{-i\pi/3}\}$.

FIG. 5. (a,d) Bulk band structures with SOC of monolayer and bilayer MoS_2. (b,e) Armchair edge states with SOC of monolayer and bilayer MoS_2. Energy discrete spectra with SOC of the finite-size triangular flakes of (c) monolayer and (f) bilayer MoS_2 calculated from the Wannier interpolation method. The corresponding charge spatial distribution of blue states in (c) and (f) plotted in their insets are well localized at the corners. The gray, red, and blue dots stand for the respective bulk, edge, and corner states. The Fermi level marked by the arrows in (c) and (f) is determined by electron counting.

We take the monolayer and bilayer MoS_2 as examples, whose nonzero topological index $\chi_{SOC}^{(3)}$ are $(-1, 2)$ and $(-2, 4)$, respectively, and the fractional corner charge $Q_{SOC}^{(3)}$ are $2e/3$ and $4e/3$, respectively. The band structures and edge states of monolayer and bilayer MoS_2 (Fig. 5) undergo some changes by the SOC effect, but the topology of these materials do not change. We calculate the discrete energy spectrum of triangular finite-size flakes, as shown in Figs. 5(c) and 5(f). There are also two groups of corner states near zero energy and with higher energy in the spectrum, similar to the spinless condition. However, the number of corner states of each group doubled compared to the spinless case. The corresponding charge distribution of corner states are plotted in their insets. Therefore, the HOTCI topology of MX_2 is also preserved in the SOC case since the large bulk band gap dominates the SOC effect. Compared with the spinless case, the corner charge will double when the SOC is taken into account (see the proof in Appendix C).

VII. CONCLUSION AND DISCUSSION

We demonstrated that C_n-symmetric large-gap HOTCIs in atomically thin group-VIB TMDs MX_2 (M = Mo, W; X = S, Se, Te) whose monolayer and few-layer samples can be prepared from the bulk counterparts by using a mechanical exfoliation technique similar to that employed for graphene [1]. The nontrivial higher-order topology of these TMDs is revealed by the nonzero topological indices and the existence of the hallmark corner states with quantized fractional charge. The C_n-symmetric HOTCIs in atomically thin group-VIB TMDs with large optical gaps (about 1.8 eV) would facilitate the experimental detection of the hallmark corner

states as sharp peaks in the scanning tunneling spectroscopy (STS) measurement, when the scanning tip approaches the corners. As the atomically thin group-VIB TMDs are easy to produce with high quality, they are ideal material candidates to explore the HOTCI states and the related remarkable properties.

When the number of layers N of the group-VIB TMDs is large, the many-layer systems will approach the 3D bulks, and we find the corner states could evolves into hinge states [64]. In addition, the planes of $k_z = 0$ and $k_z = \pi$ have the same nonzero topological indices protected by C_3 symmetry in the 3D group-VIB TMDs, which suggests that the 3D $2H$ group-VIB TMDs are C_n-symmetric higher-order weak topological crystalline insulators [64]. These contents are beyond the scope of this work and left for the next work.

Note added. We become aware of an independent work recently [65]. The work proposes second-order topological insulators in monolayer group-VIB TMDs, and the results of the monolayer group-VIB TMDs are consistent with ours.
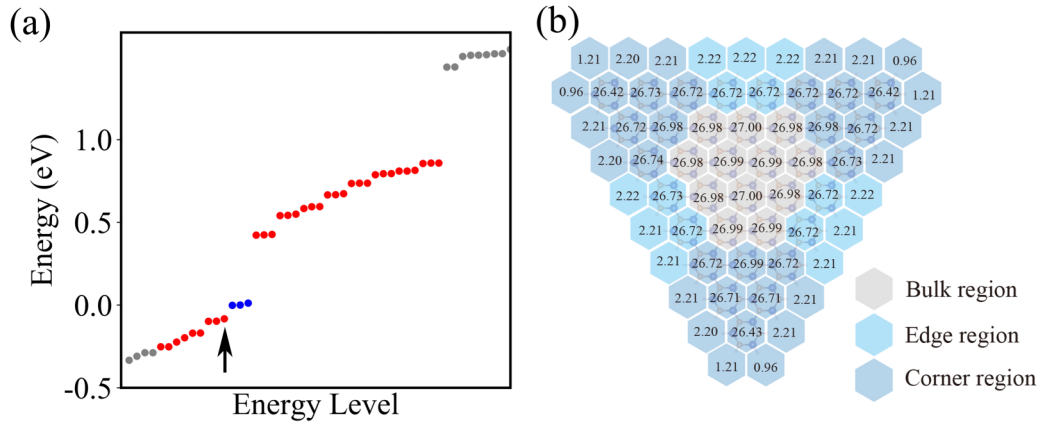
FIG. 6. (a) Energy discrete spectra of the finite-size triangular flake of monolayer MoS_2 at the edge with hydrogen passivation consisting of 108 Mo atoms, 216 S atoms and 96 H atoms calculated from VASP. The gray and blue dots represent the respective bulk and corner states. (b) Charge distribution below the corner states. The numerals in hexagonal cells denote the number of charges. The dark blue, light blue, and gray represent the corner, edge, and bulk regions, respectively.

APPENDIX A: NUMERICAL CALCULATION OF CORNER CHARGE BY VASP

The charge accumulation in the corner region is

$$Q_c = \sum_i \int_{\text{corner}} d\boldsymbol{r} |\psi_i(\boldsymbol{r})|^2 \mod 1, \qquad (A1)$$

where $|\psi_i(\boldsymbol{r})|^2$ is the charge distribution of the occupied eigenstates below the corner states and the integration is performed within the corner region. We calculated the charge distribution of charged monolayer MoS_2 at the edge with hydrogen passivation whose Fermi level is located below the corner states using VASP (Fig. 6). The charge accumulated in the corner region (the summation of the values in dark blue region in Fig. 6) mod e is about 0.30 e, which is close to the theoretical value $e/3$.

APPENDIX B: HIGHER-ORDER TOPOLOGY OF THE MULTILAYER SYSTEMS OF 2H TMDS

We take MoS_2 as an example to study the higher-order topology of the multilayer systems. Figure 7(a) shows the energy spectrum of a finite-size triangular flakes of 20-layer MoS_2 without SOC. The triangular flake consists of 45 unit cells and each unit cell has 20 layers MoS_2. Therefore it has 6300 valence electrons. The fractional corner charge is $2e/3$, the number of layers N modulo three, which is consistent with Eq. (2) of the main text. The other multilayer systems have similar results.

APPENDIX C: PROOF OF THE CORNER CHARGE DOUBLING IN ATOMICALLY THIN ($1 - N$ LAYERS) 2H TMDS WITH SOC

Since the SOC effect is not enough strong to induce a band inversion in TMDs, there is a mapping between spinless and spinful C_3 eigenvalues [28], which is

$$\begin{aligned}
\left[\tilde{K}_1^{(3)}\right] &= \left[K_1^{(3)}\right] + \left[K_2^{(3)}\right], \\
\left[\tilde{K}_2^{(3)}\right] &= \left[K_2^{(3)}\right] + \left[K_3^{(3)}\right], \qquad (C1) \\
\left[\tilde{K}_3^{(3)}\right] &= \left[K_3^{(3)}\right] + \left[K_1^{(3)}\right],
\end{aligned}$$

where $[\tilde{K}_i^{(3)}]_{i=1,2,3}$ ($[K_i^{(3)}]_{i=1,2,3}$) are the spinful (spinless) topological indices for the TMDs. From this, we obtain the relations

$$\left[\tilde{K}_1^{(3)}\right] + \left[\tilde{K}_2^{(3)}\right] = \left[K_1^{(3)}\right] + 2\left[K_2^{(3)}\right] + \left[K_3^{(3)}\right]. \qquad (C2)$$

Because the numbers of occupied bands at the reference point Γ and K are equal, $[K_1^{(3)}] + [K_2^{(3)}] + [K_3^{(3)}] = 0$. As a result, the relation between the spinless and spinful C_3 topological indices is

$$\left[\tilde{K}_1^{(3)}\right] + \left[\tilde{K}_2^{(3)}\right] = \left[K_2^{(3)}\right]. \qquad (C3)$$

The fractional corner charges for C_3-symmetry protected TMDs with SOC and without SOC are written separately as $Q_{\text{SOC}}^{(3)} = \frac{2e}{3}([\tilde{K}_1^{(3)}] + [\tilde{K}_2^{(3)}]) \mod 2e = \frac{2e}{3}[K_2^{(3)}] \mod$
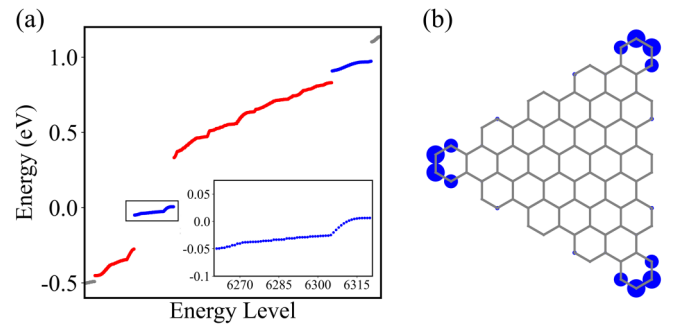

FIG. 7. (a) Energy discrete spectra of the finite-size triangular flakes of 20-layer MoS_2 without SOC. (b) The charge spatial distribution of corner states in (a). The gray, red, and blue dots represent the respective bulk, edge, and corner states.

$2e$, and $Q_{\text{corner}}^{(3)} = \frac{e}{3}[K_2^{(3)}]$ mod e [see Eqs. (3) and (1) of the main text]. Therefore, the corner charge in atomically thin

$2H$ TMDs with SOC is only a doubling of the spinless condition.

[1] K. F. Mak, C. Lee, J. Hone, J. Shan, and T. F. Heinz, Phys. Rev. Lett. **105**, 136805 (2010).

[2] A. Splendiani, L. Sun, Y. Zhang, T. Li, J. Kim, C.-Y. Chim, G. Galli, and F. Wang, Nano Lett. **10**, 1271 (2010).

[3] D. Xiao, G.-B. Liu, W. Feng, X. Xu, and W. Yao, Phys. Rev. Lett. **108**, 196802 (2012).

[4] T. Cao, G. Wang, W. Han, H. Ye, C. Zhu, J. Shi, Q. Niu, P. Tan, E. Wang, B. Liu *et al.*, Nat. Commun. **3**, 887 (2012).

[5] G.-B. Liu, D. Xiao, Y. Yao, X. Xu, and W. Yao, Chem. Soc. Rev. **44**, 2643 (2015).

[6] F. Wu, T. Lovorn, E. Tutuc, I. Martin, and A. H. MacDonald, Phys. Rev. Lett. **122**, 086402 (2019).

[7] T. P. Cysne, M. Costa, L. M. Canonico, M. B. Nardelli, R. B. Muniz, and T. G. Rappoport, Phys. Rev. Lett. **126**, 056601 (2021).

[8] M. Z. Hasan and C. L. Kane, Rev. Mod. Phys. **82**, 3045 (2010).

[9] X.-L. Qi and S.-C. Zhang, Rev. Mod. Phys. **83**, 1057 (2011).

[10] H. C. Po, A. Vishwanath, and H. Watanabe, Nat. Commun. **8**, 50 (2017).

[11] B. Bradlyn, L. Elcoro, J. Cano, M. Vergniory, Z. Wang, C. Felser, M. Aroyo, and B. A. Bernevig, Nature (London) **547**, 298 (2017).

[12] J. Kruthoff, J. de Boer, J. van Wezel, C. L. Kane, and R.-J. Slager, Phys. Rev. X **7**, 041069 (2017).

[13] M. Vergniory, L. Elcoro, C. Felser, N. Regnault, B. A. Bernevig, and Z. Wang, Nature (London) **566**, 480 (2019).

[14] F. Tang, H. C. Po, A. Vishwanath, and X. Wan, Nature (London) **566**, 486 (2019).

[15] T. Zhang, Y. Jiang, Z. Song, H. Huang, Y. He, Z. Fang, H. Weng, and C. Fang, Nature (London) **566**, 475 (2019).

[16] W. A. Benalcazar, B. A. Bernevig, and T. L. Hughes, Science **357**, 61 (2017).

[17] J. Langbehn, Y. Peng, L. Trifunovic, F. von Oppen, and P. W. Brouwer, Phys. Rev. Lett. **119**, 246401 (2017).

[18] Z. Song, Z. Fang, and C. Fang, Phys. Rev. Lett. **119**, 246402 (2017).

[19] F. Zhang, C. L. Kane, and E. J. Mele, Phys. Rev. Lett. **110**, 046404 (2013).

[20] W. A. Benalcazar, B. A. Bernevig, and T. L. Hughes, Phys. Rev. B **96**, 245115 (2017).

[21] B. Xie, H.-X. Wang, X. Zhang, P. Zhan, J.-H. Jiang, M. Lu, and Y. Chen, Nat. Rev. Phys. **3**, 520 (2021).

[22] M. Ezawa, Phys. Rev. Lett. **120**, 026801 (2018).

[23] S. Franca, J. van den Brink, and I. C. Fulga, Phys. Rev. B **98**, 201114(R) (2018).

[24] D. Călugăru, V. Juričić, and B. Roy, Phys. Rev. B **99**, 041301(R) (2019).

[25] G. van Miert and C. Ortix, Phys. Rev. B **98**, 081110(R) (2018).

[26] F. Liu, H.-Y. Deng, and K. Wakabayashi, Phys. Rev. Lett. **122**, 086804 (2019).

[27] F. Liu and K. Wakabayashi, Phys. Rev. Research **3**, 023121 (2021).

[28] F. Schindler, M. Brzezińska, W. A. Benalcazar, M. Iraola, A. Bouhon, S. S. Tsirkin, M. G. Vergniory,

and T. Neupert, Phys. Rev. Research **1**, 033074 (2019).

[29] X.-L. Sheng, C. Chen, H. Liu, Z. Chen, Z.-M. Yu, Y.-X. Zhao, and S. A. Yang, Phys. Rev. Lett. **123**, 256402 (2019).

[30] E. Lee, R. Kim, J. Ahn, and B.-J. Yang, npj Quantum Mater. **5**, 1 (2020).

[31] B. Liu, G. Zhao, Z. Liu, and Z. Wang, Nano Lett. **19**, 6492 (2019).

[32] C. Chen, W. Wu, Z.-M. Yu, Z. Chen, Y. Zhao, X.-L. Sheng, and S. A. Yang, Phys. Rev. B **104**, 085205 (2021).

[33] B. Liu, L. Xian, H. Mu, G. Zhao, Z. Liu, A. Rubio, and Z. F. Wang, Phys. Rev. Lett. **126**, 066401 (2021).

[34] M. J. Park, Y. Kim, G. Y. Cho, and S.-B. Lee, Phys. Rev. Lett. **123**, 216803 (2019).

[35] R.-X. Zhang, F. Wu, and S. Das Sarma, Phys. Rev. Lett. **124**, 136407 (2020).

[36] F. Schindler, A. M. Cook, M. G. Vergniory, Z. Wang, S. S. Parkin, B. A. Bernevig, and T. Neupert, Sci. Adv. **4**, eaat0346 (2018).

[37] Y. Xu, Z. Song, Z. Wang, H. Weng, and X. Dai, Phys. Rev. Lett. **122**, 256402 (2019).

[38] C. Yue, Y. Xu, Z. Song, H. Weng, Y.-M. Lu, C. Fang, and X. Dai, Nat. Phys. **15**, 577 (2019).

[39] C. Chen, Z. Song, J.-Z. Zhao, Z. Chen, Z.-M. Yu, X.-L. Sheng, and S. A. Yang, Phys. Rev. Lett. **125**, 056402 (2020).

[40] S. Qian, C.-C. Liu, and Y. Yao, Phys. Rev. B **104**, 245427 (2021).

[41] M. Pan, D. Li, J. Fan, and H. Huang, arXiv:2108.10823.

[42] F. Schindler, Z. Wang, M. G. Vergniory, A. M. Cook, A. Murani, S. Sengupta, A. Y. Kasumov, R. Deblock, S. Jeon, I. Drozdov *et al.*, Nat. Phys. **14**, 918 (2018).

[43] M. Serra-Garcia, V. Peri, R. Süsstrunk, O. R. Bilal, T. Larsen, L. G. Villanueva, and S. D. Huber, Nature (London) **555**, 342 (2018).

[44] H. Xue, Y. Yang, F. Gao, Y. Chong, and B. Zhang, Nat. Mater. **18**, 108 (2019).

[45] X. Ni, M. Weiner, A. Alu, and A. B. Khanikaev, Nat. Mater. **18**, 113 (2019).

[46] S. Mittal, V. V. Orre, G. Zhu, M. A. Gorlach, A. Poddubny, and M. Hafezi, Nat. Photon. **13**, 692 (2019).

[47] W. Zhang, X. Xie, H. Hao, J. Dang, S. Xiao, S. Shi, H. Ni, Z. Niu, C. Wang, K. Jin *et al.*, Light Sci. Appl. **9**, 109 (2020).

[48] J. Noh, W. A. Benalcazar, S. Huang, M. J. Collins, K. P. Chen, T. L. Hughes, and M. C. Rechtsman, Nat. Photonics **12**, 408 (2018).

[49] S. Imhof, C. Berger, F. Bayer, J. Brehm, L. W. Molenkamp, T. Kiessling, F. Schindler, C. H. Lee, M. Greiter, T. Neupert *et al.*, Nat. Phys. **14**, 925 (2018).

[50] F. Zangeneh-Nejad and R. Fleury, Phys. Rev. Lett. **123**, 053902 (2019).

[51] W. Zhang, D. Zou, Q. Pei, W. He, J. Bao, H. Sun, and X. Zhang, Phys. Rev. Lett. **126**, 146802 (2021).

[52] C. W. Peterson, W. A. Benalcazar, T. L. Hughes, and G. Bahl, Nature (London) **555**, 346 (2018).

[53] X. Zhang, B.-Y. Xie, H.-F. Wang, X. Xu, Y. Tian, J.-H. Jiang, M.-H. Lu, and Y.-F. Chen, Nat. Commun. **10**, 5331 (2019).

[54] H. Fan, B. Xia, L. Tong, S. Zheng, and D. Yu, Phys. Rev. Lett. **122**, 204301 (2019).

[55] See Supplemental Material at http://link.aps.org/supplemental/10.1103/PhysRevB.105.045417 for (i) Calculation methods; (ii) Wilson loop, nested Wilson loop, and parity criterion; (iii) bulk bands, edge states, energy spectra of triangular finite-size flakes with/without hydrogen passivation, and charge spatial distribution of corner states of the other monolayer TMDs; (iv) bulk bands, edge states, energy spectra of triangular finite-size flakes, and charge spatial distribution of corner states of the other few-layer TMDs, which includes Refs. [56–62].

[56] G. Kresse and J. Furthmüller, Phys. Rev. B **54**, 11169 (1996).

[57] J. P. Perdew, K. Burke, and M. Ernzerhof, Phys. Rev. Lett. **77**, 3865 (1996).

[58] A. A. Mostofi, J. R. Yates, Y.-S. Lee, I. Souza, D. Vanderbilt, and N. Marzari, Comput. Phys. Commun. **178**, 685 (2008).

[59] N. Marzari and D. Vanderbilt, Phys. Rev. B **56**, 12847 (1997).

[60] I. Souza, N. Marzari, and D. Vanderbilt, Phys. Rev. B **65**, 035109 (2001).

[61] Q. Wu, S. Zhang, H.-F. Song, M. Troyer, and A. A. Soluyanov, Comput. Phys. Commun. **224**, 405 (2018).

[62] J. Gao, Q. Wu, C. Persson, and Z. Wang, Comput. Phys. Commun. **261**, 107760 (2021).

[63] W. A. Benalcazar, T. Li, and T. L. Hughes, Phys. Rev. B **99**, 245151 (2019).

[64] S. Qian and C.-C. Liu (unpublished)

[65] J. Zeng, H. Liu, H. Jiang, Q.-F. Sun, and X. C. Xie, Phys. Rev. B **104**, L161108 (2021).